Article

Nonaqueous and Halide-Free Route to Crystalline BaTiO, SrTiO, and (Ba,Sr)TiO Nanoparticles via a Mechanism Involving C–C Bond Formation

Markus Niederberger, Georg Garnweitner, Nicola Pinna, and Markus Antonietti

J. Am. Chem. Soc., **2004**, 126 (29), 9120-9126• DOI: 10.1021/ja0494959 • Publication Date (Web): 29 June 2004

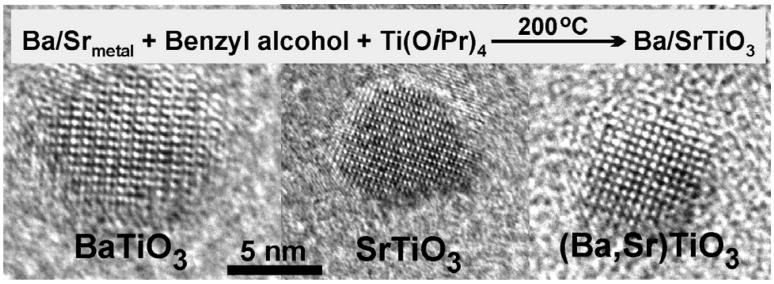

More About This Article

Additional resources and features associated with this article are available within the HTML version:

- Supporting Information
- Links to the 15 articles that cite this article, as of the time of this article download
- Access to high resolution figures
- Links to articles and content related to this article
- Copyright permission to reproduce figures and/or text from this article

View the Full Text HTML

J|A|C|S
ARTICLES
Published on Web 06/29/2004

Nonaqueous and Halide-Free Route to Crystalline $BaTiO_3$, $SrTiO_3$, and $(Ba,Sr)TiO_3$ Nanoparticles via a Mechanism Involving C−C Bond Formation

Markus Niederberger,*,† Georg Garnweitner,† Nicola Pinna,†,‡ and Markus Antonietti†

Contribution from the Max-Planck-Institute of Colloids and Interfaces, Colloid Chemistry, D-14424 Potsdam, Germany, and Department of Inorganic Chemistry, Fritz-Haber-Institute of the Max-Planck-Society, Faradayweg 4-6, D-14195 Berlin, Germany

Received January 28, 2004; E-mail: markus.niederberger@mpikg-golm.mpg.de

Abstract: A novel nonaqueous route for the preparation of nanocrystalline $BaTiO_3$, $SrTiO_3$, and $(Ba,Sr)TiO_3$ has been developed. In a simple one-pot reaction process, the elemental alkaline earth metals are directly dissolved in benzyl alcohol at slightly elevated temperatures. After the addition of $Ti(O^iPr)_4$, the reaction mixture is heated to 200 °C, resulting in the formation of a white precipitate. XRD measurements prove the exclusive presence of the perovskite phase without any other crystalline byproducts such as $BaCO_3$ or TiO_2. TEM investigations reveal that the $BaTiO_3$ nanoparticles are nearly spherical in shape with diameters ranging from 4 to 5 nm. The $SrTiO_3$ particles display less uniform particle shapes, and the size varies between 5 and 10 nm. Lattice fringes observed in HRTEM measurements further prove the high crystallinity of the nanoparticles. Surprisingly, GC−MS analysis of the reaction solution after hydrothermal treatment shows that hardly any ether formation occurs during the $BaTiO_3$ synthesis. Instead, the presence of 4-phenyl-2-butanol in stoichiometric amounts gives evidence that the formation mechanism proceeds mainly via a novel pathway involving C−C bond formation between benzyl alcohol and the isopropanolate ligand.

Introduction

Perovskite-phase mixed-metal oxides exhibit outstanding chemical and physical properties, which include catalytic, oxygen-transport, ferroelectric, pyroelectric, piezoelectric, and dielectric behavior.[1−3] Because these properties mainly depend on the crystal size, defects, surface, and interface properties, the preparation of pure, stoichiometric, homogeneous, and crystalline perovskite materials with controlled crystallite size and shape is of high interest.

Barium titanate is probably the most investigated perovskite material, because of its high dielectric constant[4−6] and ferroelectric properties[7,8] that are essential for the use in electroceramic[3,9−12] and optical materials.[13] $BaTiO_3$ exists in various crystallographic modifications, of which the tetragonal and cubic polymorphs are the most studied. The tetragonal ferroelectric structure forms in the temperature range from 0 to 130 °C, whereas the paraelectric cubic modification is stable above the Curie temperature of 130 °C. In the tetragonal polymorph, the titanium ions are distorted from the centrosymmetric position within the TiO_6 octahedra, giving rise to spontaneous polarization.[14] The polarization direction can be switched in response to an external field. The asymmetry of tetragonal $BaTiO_3$ gives rise to high permittivities, making it a promising dielectric material in multilayer and thin-film capacitors.[3,10,15−19]

Although the tetragonal polymorph is the thermodynamically stable form at room temperature, most low-temperature synthesis routes result in the formation of the cubic structure, and a high-

† Max-Planck-Institute of Colloids and Interfaces.
‡ Fritz-Haber-Institute of the Max-Planck-Society.

(1) Chandler, C. D.; Roger, C.; Hampden-Smith, M. J. *Chem. Rev.* **1993**, *93*, 1205−1241.
(2) Pena, M. A.; Fierro, J. L. G. *Chem. Rev.* **2001**, *101*, 1981−2017.
(3) Bhalla, A. S.; Guo, R.; Roy, R. *Mater. Res. Innovations* **2000**, *4*, 3−26.
(4) Dutta, P. K.; Asiaie, R.; Akbar, S. A.; Zhu, W. D. *Chem. Mater.* **1994**, *6*, 1542−1548.
(5) Her, Y.-S.; Matijevic, E.; Chon, M. C. *J. Mater. Res.* **1995**, *10*, 3106−3114.
(6) Takeuchi, T.; Tabuchi, M.; Ado, K.; Honjo, K.; Nakamura, O.; Kageyama, H.; Suyama, Y.; Ohtori, N.; Nagasawa, M. *J. Mater. Sci.* **1997**, *32*, 4053−4060.
(7) Lee, T.; Aksay, I. A. *Cryst. Growth Des.* **2001**, *1*, 401−419.
(8) Chen, Z. X.; Chen, Y.; Jiang, Y. S. *J. Phys. Chem. B* **2001**, *105*, 5766−5771.
(9) Setter, N.; Waser, R. *Acta Mater.* **2000**, *48*, 151−178.
(10) Hennings, D.; Klee, M.; Waser, R. *Adv. Mater.* **1991**, *3*, 334−340.
(11) Haertling, G. H. *J. Am. Ceram. Soc.* **1999**, *82*, 797−818.
(12) Lee, J.-Y.; Lee, J.-H.; Hong, S.-H.; Lee, Y. K.; Choi, J.-Y. *Adv. Mater.* **2003**, *15*, 1655−1658.
(13) Soten, I.; Miguez, H.; Yang, S. M.; Petrov, S.; Coombs, N.; Tetreault, N.; Matsuura, N.; Ruda, H. E.; Ozin, G. A. *Adv. Funct. Mater.* **2002**, *12*, 71−77.
(14) Clark, I. J.; Takeuchi, T.; Ohtori, N.; Sinclair, D. C. *J. Mater. Chem.* **1999**, *9*, 83−91.
(15) Frey, M. H.; Payne, D. A. *Appl. Phys. Lett.* **1993**, *63*, 2753−2755.
(16) Singh, P. K.; Cochrane, S.; Liu, W. T.; Chen, K.; Knorr, D. B.; Borrego, J. M.; Rymaszewski, E. J.; Lu, T. M. *Appl. Phys. Lett.* **1995**, *66*, 3683−3685.
(17) Kotecki, D. E.; Baniecki, J. D.; Shen, H.; Laibowitz, R. B.; Saenger, K. L.; Lian, J. J.; Athavale, S. D.; Cabral, C., Jr.; Duncombe, P. R.; Gutsche, M.; Kunkel, G.; Park, Y.-J.; Wang, Y.-Y.; Wise, R. *IBM J. Res. Dev.* **1999**, *43*, 367−382.
(18) Shaw, T. M.; Trolier-McKinstry, S.; McIntyre, P. C. *Annu. Rev. Mater. Sci.* **2000**, *30*, 263−298.
(19) Randall, C. A. *J. Ceram. Soc. Jpn.* **2001**, *109*, S2−S6.

10.1021/ja0494959 CCC: $27.50

temperature treatment at around 1000 °C is necessary to induce phase transformation from the cubic to the tetragonal structure upon cooling again to room temperature.[5,6,14] In view of the importance of the titanates, it is not surprising that a wide variety of approaches for their synthesis has been reported. In addition to coprecipitation processes[5,20−22] and pyrolysis of metallo-organic precursors,[23−25] especially sol−gel processes using titanium alkoxides and barium salts have shown to be versatile synthesis procedures,[26−31] often in the presence of organic species that act either as complexing agent for the barium ions[32] or as stabilizing agent to prevent agglomeration of the particles.[33−35] Another frequently applied process is the hydrothermal treatment of a titania source, such as titanium alkoxide, titanium oxide, or titanium oxide gels, in the presence of barium salts such as barium halides, acetate, nitrate, or hydroxide in strongly alkaline solutions.[14,36−39] The anions of the barium salt as well as the hydroxide concentrations have a strong influence on the cubic-to-tetragonal polymorph ratio in the final material.[4,40] The use of a stearic acid sol−gel technique allowed the synthesis of photoluminescent nanocrystalline $SrTiO_3$,[41] whereas the reaction between TiO_2 anatase and strontium oxalate in the presence of nonylphenyl ether results in the formation of single-crystalline $SrTiO_3$ nanocubes.[42]

Many of the physical properties of perovskite materials are critically dependent on the particle size as well as on the dimensionality. Because one-dimensional nanoparticles exhibit unique properties due to the size confinement in the radial direction,[43] a wide variety of synthesis methods for the preparation of $BaTiO_3$ and $SrTiO_3$ nanotubes and nanowires has been reported. The solution-phase decomposition of bimetallic alkoxide precursors in the presence of coordinating ligands yielded well-isolated and single-crystalline nanorods[44] and nanowires.[45,46] Combination of sol−gel processing and electrophoretic deposition yielded perovskite nanorods,[47] and the use of titania nanotubes or TiO_2 anatase as precursor material resulted in the formation of crystalline perovskite nanotubes[48] or nanowires.[42] All of these preparation methods lead to the formation of particle sizes in the range of a few hundred to a few tens of nanometers. However, $BaTiO_3$ particles smaller than 10 nm and nearly spherical in shape are of particular interest for several reasons. First, nanocrystalline $BaTiO_3$ is, in contrast to the bulk material, nonferroelectric and stabilized in the cubic structure at room temperature, resulting in stable dielectric properties.[6,15,16] There is still no clear consensus about the origin of this so-called size effect,[14] although several explanations have been proposed.[18,49] A simple synthesis route to nanocrystalline $BaTiO_3$ in gram quantities would facilitate further investigations on the precise nature of ferroelectricity in the dependence of the particle size. Another important reason for having $BaTiO_3$ in a nanocrystalline form is the current trend to miniaturization in the fabrication of nanodevices with improved properties and high reliability. For all of these applications, it is a key requirement that the $BaTiO_3$ powder can easily be processed into defect-free thin films,[9,10,18,30,50,51] and, thus, small crystallite sizes and high purity and compositional homogeneity are important prerequisites. Furthermore, powders with uniform and fine particle size provide good sinterability, an essential property for the formation of advanced ceramic materials.[3,11]

Here, we report a novel innovative reaction approach employing a nonhydrolytic and halide-free procedure to synthesize nanocrystalline $BaTiO_3$, $SrTiO_3$, and $(Ba,Sr)TiO_3$ particles with diameters ranging typically from 4 to 10 nm.[52,53] The reaction between titanium isopropoxide and barium or strontium metal dissolved in benzyl alcohol results in the formation of $BaTiO_3$, $SrTiO_3$, and $(Ba,Sr)TiO_3$ mixed oxide nanoparticles. Benzyl alcohol has already shown to be a versatile reaction medium for the synthesis of transition metal oxide nanoparticles with good control over particle size, shape, crystallinity,[54,55] solubility,[56] and assembly behavior.[57] Without the use of any additional ligands or templates, the crystal growth is highly controlled. Furthermore, the use of the alkaline earth metals and titanium isopropoxide in benzyl alcohol is a particularly attractive reaction system for several more reasons: (i) phase-pure $BaTiO_3$ is obtained without other byproducts such as barium carbonate, and, therefore, subsequent separation steps can be avoided; (ii) all precursors are commercially available; (iii) the reaction is a

(20) Hu, M. Z.-C.; Miller, G. A.; Payzant, E. A.; Rawn, C. J. *J. Mater. Sci.* **2000**, *35*, 2927−2936.
(21) Wada, S.; Tsurumi, T.; Chikamori, H.; Noma, T.; Suzuki, T. *J. Cryst. Growth* **2001**, *229*, 433−439.
(22) Xu, H. R.; Gao, L. *J. Am. Ceram. Soc.* **2003**, *86*, 203−205.
(23) Duran, P.; Capel, F.; Gutierrez, D.; Tartaj, J.; Banares, M. A.; Moure, C. *J. Mater. Chem.* **2001**, *11*, 1828−1836.
(24) Rumpf, H.; Modrow, H.; Hormes, J.; Glasel, H. J.; Hartmann, E.; Erdem, E.; Bottcher, R.; Hallmeier, K. H. *J. Phys. Chem. B* **2001**, *105*, 3415−3421.
(25) Arya, P. R.; Jha, P.; Ganguli, D. *J. Mater. Chem.* **2003**, *13*, 415−423.
(26) Frey, M. H.; Payne, D. A. *Chem. Mater.* **1995**, *7*, 123−129.
(27) Viswanath, R. N.; Ramasamy, S. *Nanostruct. Mater.* **1997**, *8*, 155−162.
(28) Khalil, K. M. S. *Mater. Res. Innovations* **1999**, *2*, 256−262.
(29) Special Issue "Sol-Gel Processing of Ferroelectric Materials". *J. Sol.-Gel Sci. Technol.* **1999**, *16*.
(30) Matsuda, H.; Kobayashi, N.; Kobayashi, T.; Miyazawa, K.; Kuwabara, M. *J. Non-Cryst. Solids* **2000**, *271*, 162−166.
(31) Hung, K. M.; Yang, W. D.; Huang, C. C. *J. Eur. Ceram. Soc.* **2003**, *23*, 1901−1910.
(32) Gherardi, P.; Matijevic, E. *Colloids Surf.* **1988**, *32*, 257−274.
(33) O'Brien, S.; Brus, L.; Murray, C. B. *J. Am. Chem. Soc.* **2001**, *123*, 12085−12086.
(34) Lee, T.; Yao, N.; Imai, H.; Aksay, I. A. *Langmuir* **2001**, *17*, 7656−7663.
(35) Wu, X.; Zou, L.; Yang, S.; Wang, D. *J. Colloid Interface Sci.* **2001**, *239*, 369−373.
(36) Dutta, P. K.; Gregg, J. R. *Chem. Mater.* **1992**, *4*, 843−846.
(37) Walton, R. I.; Millange, F.; Smith, R. I.; Hansen, T. C.; O'Hare, D. *J. Am. Chem. Soc.* **2001**, *123*, 12547−12555.
(38) Ciftci, E.; Rahaman, M. N.; Shumsky, M. *J. Mater. Sci.* **2001**, *36*, 4875−4882.
(39) Zhang, M.-S.; Yu, J.; Chu, J.; Chen, D.; Chen, W. *J. Mater. Process. Technol.* **2003**, *137*, 78−81.
(40) Asiaie, R.; Zhu, W. D.; Akbar, S. A.; Dutta, P. K. *Chem. Mater.* **1996**, *8*, 226−234.
(41) Zhang, W. F.; Yin, Z.; Zhang, M. S.; Du, Z. L.; Chen, W. C. *J. Phys.: Condens. Matter* **1999**, *11*, 5655−5660.
(42) Mao, Y. B.; Banerjee, S.; Wong, S. S. *J. Am. Chem. Soc.* **2003**, *125*, 15718−15719.
(43) Hu, J. T.; Odom, T. W.; Lieber, C. M. *Acc. Chem. Res.* **1999**, *32*, 435−445.
(44) Urban, J. J.; Yun, W. S.; Gu, Q.; Park, H. *J. Am. Chem. Soc.* **2002**, *124*, 1186−1187.
(45) Yun, W. S.; Urban, J. J.; Gu, Q.; Park, H. *Nano Lett.* **2002**, *2*, 447−450.
(46) Urban, J. J.; Spanier, J. E.; Lian, O. Y.; Yun, W. S.; Park, H. *Adv. Mater.* **2003**, *15*, 423−426.
(47) Limmer, S. J.; Seraji, S.; Wu, Y.; Chou, T. P.; Nguyen, C.; Cao, G. Z. *Adv. Funct. Mater.* **2002**, *12*, 59−64.
(48) Mao, Y. B.; Banerjee, S.; Wong, S. S. *Chem. Commun.* **2003**, 408−409.
(49) Frey, M. H.; Xu, Z.; Han, P.; Payne, D. A. *Ferroelectrics* **1998**, *206*, 337−353.
(50) Wang, M. C.; Hsiao, F. Y.; Hsi, C. S.; Wu, N. C. *J. Cryst. Growth* **2002**, *246*, 78−84.
(51) Zhang, J.; Yin, Z.; Zhang, M.-S. *Phys. Lett. A* **2003**, *310*, 479−485.
(52) Antonietti, M.; Niederberger, M. *Deutsche Patentanmeldung* **2003**, *Nr. 10338465.0*.
(53) Niederberger, M.; Pinna, N.; Polleux, J.; Antonietti, M. *Angew. Chem., Int. Ed.* **2004**, *43*, 2270−2273.
(54) Niederberger, M.; Bartl, M. H.; Stucky, G. D. *J. Am. Chem. Soc.* **2002**, *124*, 13642−13643.
(55) Niederberger, M.; Bartl, M. H.; Stucky, G. D. *Chem. Mater.* **2002**, *14*, 4364−4370.
(56) Niederberger, M.; Garnweitner, G.; Krumeich, F.; Nesper, R.; Cölfen, H.; Antonietti, M. *Chem. Mater.* **2004**, *16*, 1202−1208.
(57) Polleux, J.; Pinna, N.; Antonietti, M.; Niederberger, M. *Adv. Mater.* **2004**, *16*, 436−439.

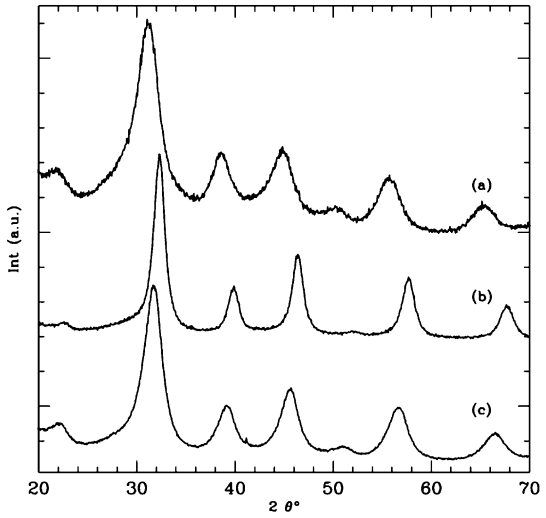

Figure 1. XRD powder patterns of (a) $BaTiO_3$, (b) $SrTiO_3$, and (c) $Ba_{0.5}Sr_{0.5}TiO_3$. All reflections can be assigned to the respective perovskite phase without other crystalline byproducts.

simple, low-temperature process; (iv) the yields can easily be scaled-up; and (v) there is by concept no contamination with other inorganics such as halides or alkali metal ions, which are difficult to remove from the final perovskite material. The formation of the $BaTiO_3$ nanoparticles occurs via an unprecedented reaction pathway involving C−C bond formation between benzyl alcohol and the isopropanolate ligand.

Results and Discussion

In the first step of the synthesis performed in a glovebox, metallic barium and/or strontium is dissolved in anhydrous benzyl alcohol at elevated temperature (70−100 °C). Generally, strontium needs a higher temperature to dissolve than barium. Highly electropositive elements such as alkali metals and alkaline earth metals react directly with alcohols under release of hydrogen and the formation of alkoxides.[58] In the case of alkaline earth metals, the insolubility of the bivalent alkoxides often becomes a problem. Here, barium and strontium form completely transparent and, in the case of barium, slightly yellowish solutions in benzyl alcohol. After the addition of 1 mol equivalent of titanium isopropoxide, the reaction mixture is transferred to a steel autoclave and heated in a furnace at 200 °C for 48 h. It is interesting to note that 200 °C is still below the boiling point of benzyl alcohol (205 °C). Therefore, the reaction takes place under subsolvothermal conditions. However, if the reaction is performed in an open reaction vessel at 200 °C under ambient pressure, only a white precipitate mainly amorphous in nature is formed rather than crystalline perovskite nanoparticles.

Typical X-ray powder diffraction (XRD) patterns of as-synthesized perovskite powders are given in Figure 1. All diffraction peaks in Figure 1a can be assigned to the $BaTiO_3$ phase (JCPDS No. 31-174) without any indication of crystalline byproducts such as $BaCO_3$ or TiO_2. The powder pattern in the 40−50° 2θ region is usually characteristic for the presence of either the cubic or the tetragonal $BaTiO_3$ structure.[59] However, in the present case, due to the small particle size the reflections are too broad to discriminate between the two crystal modifications.[53] The XRD patterns of $SrTiO_3$ and of the mixed oxide $Ba_{0.5}Sr_{0.5}TiO_3$ are shown in Figure 1b and c, respectively. All reflections match well with the respective crystal structure (JCPDS No. 35-734 for $SrTiO_3$ and JCPDS No. 39-1395 for $Ba_{0.5}Sr_{0.5}TiO_3$), without the presence of any carbonate peaks. With increasing amount of Sr, the reflection positions shift to higher diffraction angles, as it is expected from the smaller lattice constants caused by the substitution of the larger Ba ions by the smaller Sr ions. For example, the 101/110 reflection shifts from $2\theta = 31.19$ ($BaTiO_3$) to 31.69 ($Ba_{0.5}Sr_{0.5}TiO_3$) and 32.31 ($SrTiO_3$). This proves that it is also possible to obtain the mixed oxides by this synthesis approach.

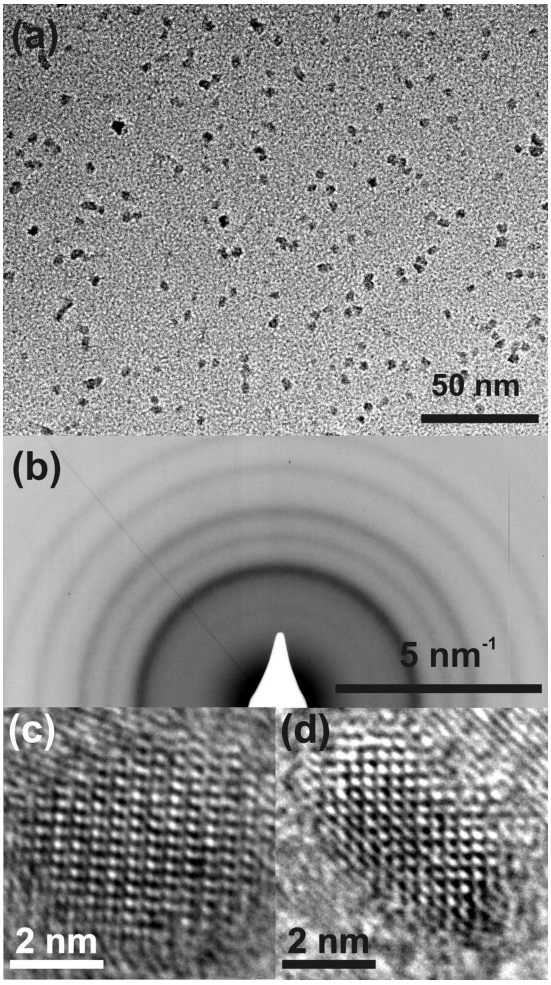

Figure 2. Representative TEM micrographs of as-synthesized $BaTiO_3$ nanoparticles. (a) An overview image proves the exclusive presence of $BaTiO_3$ nanoparticles without the presence of larger particles or agglomerates; (b) selected area electron diffraction (SAED); (c) and (d) high-resolution TEM images of isolated $BaTiO_3$ nanocrystals.

Representative transmission electron micrographs (TEM) of the barium titanate sample are shown in Figure 2. An overview image (Figure 2a) at low magnification illustrates that the sample entirely consists of nanosized individual barium titanate particles without the presence of larger particles or agglomerates. Crystallinity and phase are confirmed by electron diffraction analysis, revealing diffraction rings typical for the barium titanate phase (Figure 2b). Images of isolated nanocrystals at higher magnification (HRTEM, Figure 2c and d) show sets of lattice fringes, giving additional evidence that the particles are highly crystalline. The particles are quite uniform in size and

(58) Mehrotra, R. C.; Singh, A.; Sogani, S. *Chem. Soc. Rev.* **1994**, *23*, 215−225.
(59) Frey, M. H.; Payne, D. A. *Phys. Rev. B* **1996**, *54*, 3158−3168.

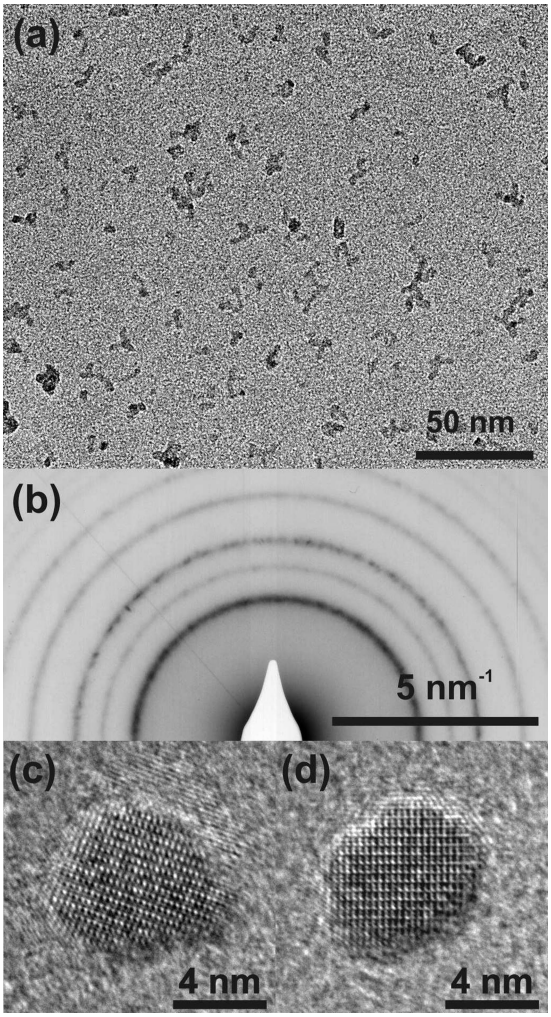

Figure 3. Representative TEM micrographs of as-synthesized $SrTiO_3$ nanoparticles. (a) Overview; (b) selected area electron diffraction (SAED); (c) and (d) high-resolution TEM images of isolated $SrTiO_3$ nanocrystals.

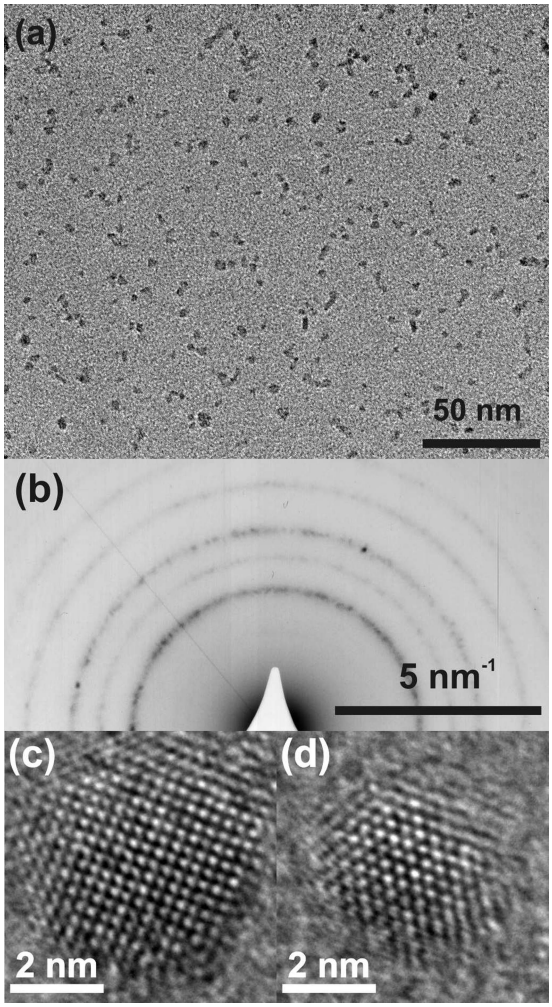

Figure 4. Representative TEM micrographs of as-synthesized $Ba_{0.5}Sr_{0.5}TiO_3$ nanoparticles. (a) Overview; (b) selected area electron diffraction with diffraction rings corresponding to the $Ba_{0.5}Sr_{0.5}TiO_3$ phase; (c) and (d) high-resolution TEM images of isolated $Ba_{0.5}Sr_{0.5}TiO_3$ nanocrystals.

shape and mostly spherical. Typically, the particle diameter ranges from 4 to 5 nm.

Figure 3 shows TEM images of $SrTiO_3$. According to the overview image (Figure 3a), the particle size and shape is less uniform than in the case of the $BaTiO_3$ sample. The particle size typically varies between 5 and 10 nm. In addition to nearly spherical particles, also elongated particles are found. The SAED pattern (Figure 3b) shows that the particles are highly crystalline, and the diffraction rings match with the strontium titanate structure. HRTEM images of isolated nanoparticles (Figure 3c and d) point out the good crystallinity and give evidence for the absence of structural defects. Both particles are oriented along the [110] direction.

TEM images of the mixed oxide $Ba_{0.5}Sr_{0.5}TiO_3$ are displayed in Figure 4. In contrast to the pure $SrTiO_3$ phase, the particles exhibit a more uniform size and shape. In most cases, the particles have a spherical shape with an average diameter of about 5 nm (Figure 4a). The *d* spacings measured from the diffraction rings of the SAED pattern (Figure 4b) are in good agreement with the cubic $Ba_{0.5}Sr_{0.5}TiO_3$ structure. HRTEM images of isolated nanoparticles (Figure 4c and d) show several lattice planes, giving additional evidence that the particles are highly crystalline. The particles are oriented along the [100] (Figure 4c) and [111] direction (Figure 4d), respectively. Energy-dispersive X-ray analysis (EDX) has been used to probe the composition of the $Ba_{0.5}Sr_{0.5}TiO_3$ nanoparticles. Because the Ba L-edge and the Ti K-edge overlap in the energy range of 4.5−5 keV, it is not possible to determine the composition of the sample quantitatively. However, Ba as well as Sr were detected in the sample, giving additional evidence for the mixed-phase oxide.

Nonhydrolytic pathways to titania mainly involve the reaction of titanium tetrachloride with either a metal alkoxide or an organic oxygen donor such as diisopropyl ether.[60] In these routes, the formation of the Ti−O−Ti bonds results from the condensation between Ti−Cl and M−OR functions, where M is either a titanium atom[61,62] or an organic alkyl group.[60,63] However, in our reaction system, there are no halides present. A possible reaction pathway for halide-free systems involves an aprotic condensation reaction, where the formation of an oxo bridge is provided by eliminating an organic ether:[63]

(60) Arnal, P.; Corriu, R. J. P.; Leclercq, D.; Mutin, P. H.; Vioux, A. *Chem. Mater.* **1997**, *9*, 694−698.
(61) Trentler, T. J.; Denler, T. E.; Bertone, J. F.; Agrawal, A.; Colvin, V. L. *J. Am. Chem. Soc.* **1999**, *121*, 1613−1614.
(62) Corriu, R. J. P.; Leclercq, D.; Lefevre, P.; Mutin, P. H.; Vioux, A. *J. Mater. Chem.* **1992**, *2*, 673−674.
(63) Vioux, A. *Chem. Mater.* **1997**, *9*, 2292−2299.

$$\equiv M-OR + RO-M\equiv \rightarrow \equiv M-O-M\equiv + R-O-R$$

This ether elimination route might take place in the formation of a mixed-metal oxoalkoxide obtained from the reaction between titanium isopropoxide and lead isopropoxide.[64] Yet, in any case, this process is rarely employed as compared to the ester and alkyl halide eliminations.[63]

To elucidate the reaction mechanism of the $BaTiO_3$ nanoparticle formation, a synthesis was performed with a particularly small amount of benzyl alcohol (ratio of benzyl alcohol to Ba of 7) to facilitate the identification of the formed organic compounds. The reaction mixture was centrifuged to remove the $BaTiO_3$ precipitate, and the supernatant liquid additionally filtered and then analyzed by ^1H, ^{13}C NMR spectroscopy and by coupled gas chromatography−mass spectrometry (GC−MS).

Figure 5 shows some results of the gas chromatography measurements for the filtered reaction mixture. Signal **1** corresponds to isopropanol, and **2** stems from hexane used as solvent for the chromatography (the main hexane peak was blinded out). The mass spectrum of peak **3** can be clearly assigned to toluene, and peak **4** can be assigned to benzyl alcohol. The assignment of signal **5**, representing the main product, is discussed below. Peak **6** is identified as 1,5-diphenyl-3-pentanol. The signals **5*** and **6*** correspond to the ketones 4-phenyl-2-butanone and 1,5-diphenyl-3-pentanone, respectively. It is interesting to note that the initially expected organic ethers such as benzyl ether, isopropyl ether, and benzyl isopropyl ether are found only in minor quantities.

The recorded mass spectrum of peak **5** is shown in Figure 5, inset. The spectrum matches well with that of 4-phenyl-2-butanol. The M^+ peak appears at *m*/*z* 150, whereas the peak at *m*/*z* 132 corresponds to the dehydrated fragment $[M - H_2O]^+$. Cleavage of the α′-methyl group and additional dehydration leads to *m*/*z* 117. The *m*/*z* 91 signal can be assigned to the stabilized benzyl fragment $[C_7H_7]^+$. The less favored α-cleavage leads to the peaks at *m*/*z* 105 and *m*/*z* 45, whereas *m*/*z* 78 corresponds to the phenyl fragment. The spectrum is in excellent accordance with reference spectra for 4-phenyl-2-butanol found in the Integrated Spectral Data Base System for Organic Compounds.[65]

The reaction mixture was also analyzed by ^{13}C NMR spectroscopy (Figure 6). Benzyl alcohol is present in excess; therefore, the corresponding peaks (labeled **BA**) are dominant. The unsubstituted aromatic carbon atoms appear at 126.9−128.3 ppm, whereas the aliphatic peak is visible at 64.8 ppm. Isopropanol causes the prominent peak at 25.3 ppm; the signal of the secondary carbon (expected at 64.0 ppm) is superimposed by the benzyl alcohol peak, but it is still visible as a shoulder. All peaks of the main reaction product, 4-phenyl-2-butanol, can be seen in the spectrum. However, the aromatic carbon atoms labeled **6** appear at positions very close to the BA peaks, leading to the signal at 125.5−128.5 ppm. The substituted aromatic position (peak **5**) appears now at 142.6 ppm, which constitutes further deshielding (as compared to 141.5 ppm for the corresponding position in benzyl alcohol) caused by the larger alkyl moiety bound to the aromatic system. The aliphatic peaks are nicely visible at 23.6, 32.3, 41.0, and 67.3 ppm (peaks **1**−**4**).

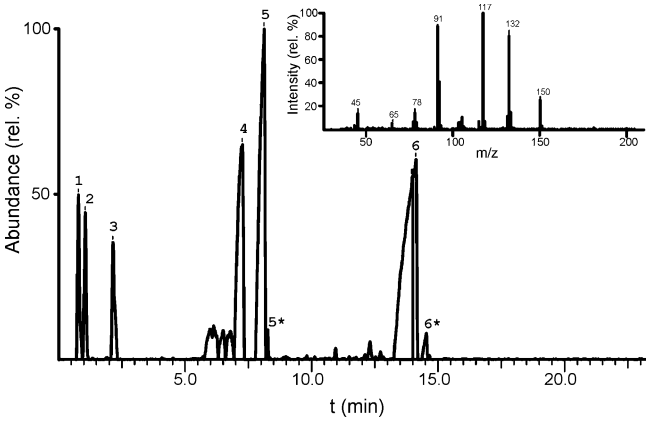

Figure 5. Gas chromatogram of the final reaction solution after filtration; inset: mass spectrum of peak **5**.

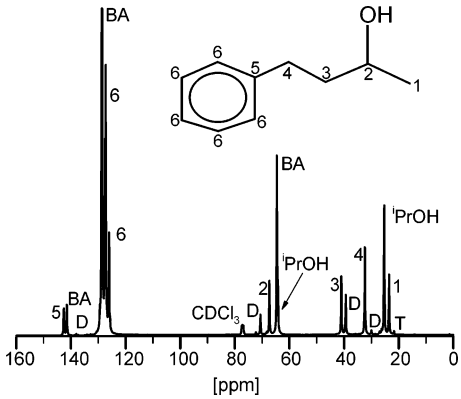

Figure 6. BB-decoupled ^{13}C NMR spectrum of the filtered reaction solution measured in $CDCl_3$.

The peaks marked **D** are likely to be caused by the disubstituted product 1,5-diphenyl-3-pentanol, as verified in NMR simulations, whereas the peak marked **T** at 21.4 ppm can be clearly attributed to toluene. The ketone products identified in GC−MS measurements could not be detected in the NMR spectrum due to their small amount in the reaction solution.

These results are surprising, because it was expected that nonaqueous condensation reactions between metal alkoxides and alcohols should occur via an ether elimination pathway.[63] Furthermore, to the best of our knowledge, up to now there is no reaction known in metal-organic chemistry leading to the formation of an alkyl C−C bond between an alcohol and the β-position of a simple metal alkoxide. However, it has been known for years that C−H bonds can be activated by the coordination of organic molecules to metal centers,[66] and a great deal of research has been carried out to study these activations.[67] Aldol addition, one of the most prominent reactions to form C−C bonds, can be catalyzed and even stereochemically controlled by using titanium alkoxides.[68−70] Only recently, there has been one report of the direct reaction of $Ti(O^tBu)_4$ with aldehydes leading to the formation of diols and triols under the influence of lithium salts, and barium salts were reported to react similarly;[71] however, these results were corrected later.[72]

(64) Daniele, S.; Papiernik, R.; Hubert-Pfalzgraf, L. G.; Jagner, S.; Hakansson, M. *Inorg. Chem.* **1995**, *34*, 628−632.
(65) Integrated Spectral Data Base System for Organic Compounds: http://www.aist.go.jp/RIODB/SDBS/.
(66) Dawoodi, Z.; Green, M. L. H.; Mtetwa, V. S. B.; Prout, K. *J. Chem. Soc., Chem. Commun.* **1982**, 802−803.
(67) Labinger, J. A.; Bercaw, J. E. *Nature* **2002**, *417*, 507−514.
(68) Reetz, M. T.; Peter, R. *Tetrahedron Lett.* **1981**, *22*, 4691−4694.
(69) Mahrwald, R. *Tetrahedron* **1995**, *51*, 9015−9022.
(70) Mahrwald, R. *Org. Lett.* **2000**, *2*, 4011−4012.
(71) Mahrwald, R. *Angew. Chem., Int. Ed.* **2002**, *41*, 1361−1363.

Scheme 1. Proposed Reaction Mechanism for the Simultaneous Formation of $BaTiO_3$ Nanoparticles and 4-Phenyl-2-butanol

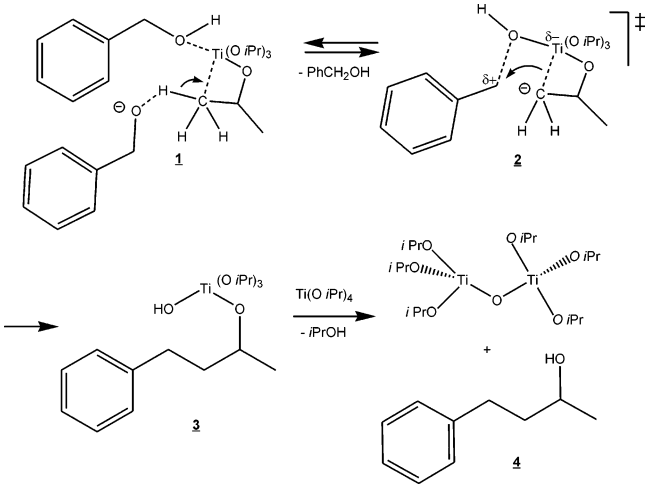

Scheme 2. Suggestion of a Side Reaction Mechanism, Somewhat Similar to the Meerwein−Ponndorf−Verley Reduction, Leading to the Formation of Toluene and 4-Phenyl-2-butanone

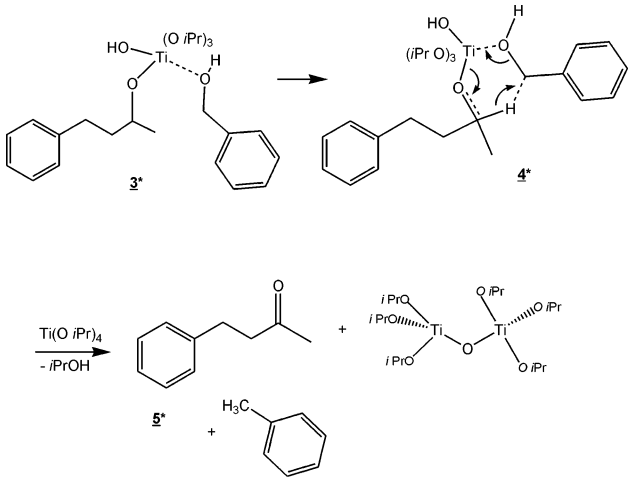

The importance of the titanium species in our reaction pathway is further supported by the fact that two reference experiments without titanium isopropoxide, the reaction of benzyl alcohol with isopropanol and the reaction of metallic barium in benzyl alcohol with isopropanol under similar reaction conditions, do not at all or only to a much smaller extent result in the formation of 4-phenyl-2-butanol.

We propose a reaction mechanism according to Scheme 1. The resulting C−C bond can conceivably only be formed via a nucleophilic attack of a β-carbon atom of the isopropoxide onto the benzyl group which is activated by an interaction of the alcohol −OH group with Ti. Hence, in the first step, benzyl alcohol is assumed to coordinate to a Ti atom, forming a five-fold coordination complex. Upon coordination, the C−O bond of the benzyl alcohol is weakened, and the resulting benzylic carbon atom is highly activated toward nucleophilic attack. In the next step, one of the two β-carbon atoms of the isopropoxy group is formally deprotonated (**1**). The role of the base is most probably played by the benzyl alcoholate, which was produced from the reaction between metallic Ba and benzyl alcohol. This is supported by the fact that the formation of 4-phenyl-2-butanol occurs only in the presence of Ba. It is a notable feature of this reaction that deprotonation does not occur on the α-carbon atom, but on the β-sites, only. This means that the deprotonation is supported by a stabilizing effect of the C−Ti interaction, as indicated by the dashed line (**2**). This interaction, similar to an agostic bond,[66] leads to a coordinatively saturated, hexa-coordinated Ti center. Due to the sterical proximity of the benzyl group and the formal carbanion at two neighboring sites of the intermediate titanium octahedron, the nucleophilic attack is expected to occur quite fast, resulting in the formation of a titanium complex with a coordinated 4-phenyl-2-butoxide (**3**) and an OH-group. This OH-group later on promotes further condensation of the titanium monomer to the Ti−O−Ti species via alcohol elimination, finally leading to the oxidic nanoparticles. To the same degree as the inorganic crystal formation, this process leads to the release of the alcohol (**4**). The presence of smaller amounts of 1,5-diphenyl-3-pentanol in the reaction mixture shows that also the other methyl group of the isopropoxide ligand can react with another benzyl group in an analogous manner; however, due to the sterical hindrance this reaction is at lower reaction rates.

According to ^{1}H NMR measurements (see Supporting Information), the final molar ratio of 4-phenyl-2-butanol to ^{i}PrOH is approximately 0.75 to 1, whereas the postulated mechanism would lead to a ratio of 1. This speaks for the high efficiency of the reaction pathway and the coupled high yields; the differences are presumably due to the existence of another, also novel, side reaction. The presence of toluene in the final solution gives evidence that this side reaction most probably involves a hydride transfer, similar to the Meerwein−Ponndorf−Verley (MPV) reaction. The absence of acetone in the system shows that oxidation of an isopropoxide group does not occur. However, higher ketones such as 4-phenyl-2-butanone and 1,5-diphenyl-3-pentanone have been detected in the system by GC−MS.

Scheme 2 gives a possible mechanism of this side reaction of toluene and ketone formation starting with complex **3** from Scheme 1. In a first step, another benzyl alcohol molecule coordinates to the titanium, once again creating a strongly electrophilic benzylic carbon atom. The next reaction step (**4***) involves a hydride transfer from the α-carbon atom, similar to the MPV reduction. The main difference of a MPV reaction, however, is that no aldehyde or ketone was used. Here, the reduction of benzyl alcohol by oxidation of another, 4-phenyl-2-butanol, resulted in the formation of toluene and 4-phenyl-2-butanone (**5***). Of course, also for this reaction a mediating influence of Ba^{2+} ions is possible. 1,5-Diphenyl-3-pentanone is assumed to form in a similar way starting from Ti-coordinated 1,5-diphenyl-3-pentanol. The obtained ratio of diphenyl ketones to monophenyl ketones was much higher than the ratio of 1,5-diphenyl-3-pentanol to 4-phenyl-2-butanol, suggesting that the hydride transfer is preferred for those species through stabilization effects of the benzyl substitution; that is, 1,5-diphenyl-3-pentanol is the better reducing agent. This view also explains the strict absence of acetone in the system. The molar ratio of toluene to 4-phenyl-2-butanol in the final solution was calculated from ^{1}H NMR to be about 1:6. This finding explains half of the missing yield of 4-phenyl-2-butanol.

Vice versa, the strong but reversible binding of titanium to the different aromatic alcohols also explains the extraordinary quality and high colloidal stability of the final oxidic nanoparticles.

(72) Mahrwald, R. *Angew. Chem., Int. Ed.* **2003**, *42*, 2443.

It is to be assumed that their surface is tightly covered with these alcohols, presumably via unhydrolyzed Ti−O−R groups.

Conclusion

The direct use of the alkaline earth metals barium and strontium together with titanium alkoxides in benzyl alcohol provides a comfortable route to crystalline perovskite nanoparticles. The complete absence of any halide precursors and other inorganics such as alkali metal ions allows the synthesis of a high-purity material. The reaction proceeds via a novel pathway involving C−C bond formation between the benzyl alcohol and the isopropanolate of the titanium alkoxide and, thus, extends the available nonaqueous reaction methodologies in addition to the well-known ester and alkyl halide eliminations. The new approach is a simple, one-pot procedure using commercially available precursors and enables the cheap and gram production of crystalline $BaTiO_3$, $SrTiO_3$, and $(Ba,Sr)TiO_3$ nanoparticles in the sub-10 nm size range.

Experimental Section

Materials. Titanium(IV) isopropoxide (99.999%), barium (99.99%) and strontium metal (99.99%), and anhydrous benzyl alcohol (99.8%) were obtained from Aldrich. All of the chemicals were used without further purification. For the hydrothermal treatment, we used Parr acid digestion bombs with 45 mL Teflon cups.

Synthesis. The whole procedure was carried out in a glovebox. In a typical synthesis, 2 mmol of the alkaline earth metal (274.7 mg of Ba or 175.2 mg of Sr) was stirred in a vial with 25 mL of benzyl alcohol at slightly elevated temperature until completely dissolved. For the $(Ba,Sr)TiO_3$, 1 mmol of Ba and 1 mmol of Sr were dissolved together in the benzyl alcohol. Next, 1 mol equivalent of $Ti(O^iPr)_4$ was added dropwise to the solution. The reaction mixture was stirred for another few minutes and then transferred into the autoclave. The autoclave was taken out of the glovebox and heated to 200 °C for about 48 h. The resulting milky suspension was centrifuged, and the precipitate was thoroughly washed with ethanol and diethyl ether and subsequently dried in air at 60 °C overnight. The yield of the as-synthesized white perovskite powder was about 90%.

For the analysis of the reaction mixture by GC−MS, ^1H, and ^{13}C NMR, the concentration of benzyl alcohol was decreased: 502.8 mg of Ba was dissolved in 5 mL of benzyl alcohol, resulting in a yellow, slightly cloudy solution. After the addition of 1 mol equivalent of $Ti(O^iPr)_4$, the orange liquid was treated hydrothermally at 200 °C for 48 h. The reaction mixture was centrifuged, and the precipitate was filtered off. The transparent reaction solution was analyzed by GC−MS and NMR, and the precipitate was analyzed by XRD. The reference experiments without $Ti(O^iPr)_4$ were performed under similar conditions, but to avoid any effects from impurities new Teflon cups were used.

Characterization. The X-ray powder diffraction (XRD) diagrams of all samples were measured in the reflection mode (Cu Kα radiation) on a Bruker D8 diffractometer equipped with a scintillation counter. XRD patterns were obtained for 20−80° 2θ by step-scanning with a step size of 0.01°. Transmission electron microscopy (TEM) investigations were performed on a CM200 FEG (Philips) microscope, operated at 200 kV (HRTEM). The samples were deposited onto a perforated carbon foil supported on a copper grid. NMR analysis was performed on a Bruker DPX400 spectrometer at 400 MHz for ^1H and 100 MHz for ^1H BB-decoupled ^{13}C measurements, at a sample spinning rate of 20 Hz, and with a ZG30 pulse program. GC−MS analysis was performed on a Varian Series 3400 gas chromatograph equipped with a 30 m × 0.25 mm i.d. fused-silica column coated with a 0.25 μm film of DB5 poly(5% diphenyl−95% dimethylsiloxane) from J&W Scientific. Helium was used as carrier gas (flow rate of 1 mL/min), and ca. 1 μL of the sample diluted with hexane was injected. The injector temperature was 270 °C. The oven temperature was maintained isothermal at 50 °C for 1 min, and then increased by 20°/min from 50 to 250 °C, which was held isothermal for 10 min. The gas chromatograph was coupled directly to a SSQ 710 quadrupole MS by Finnigan. The interface temperature was 320 °C, the ion source temperature was 150 °C, the electron energy was 70 eV, the filament current was 200 μA, and the scan rate of the mass spectrometer was 1.0 s/scan over the m/z range of 50−700. Methane-chemical ionization mass spectra were recorded with a source temperature of 120 °C and a source pressure 1 × 10^3 Pa.

Acknowledgment. Financial support by the Max-Planck-Society is gratefully acknowledged. GC−MS measurements were carried out by I. Starke, Chemisches Institut der Universität Potsdam, Karl-Liebknecht-Strasse 24-25, D-14476 Golm, Germany, and we thank I. Starke for helpful discussions. We also thank Dr. Bernd Smarsly for helpful discussions concerning the XRD data.

Supporting Information Available: ^1H NMR spectrum of the filtered reaction solution. This material is available free of charge via the Internet at http://pubs.acs.org.

JA0494959